etration into a layer of warm ice. Furthermore, the 50% melt contour would completely penetrate a 3-km-thick layer of ice overlying liquid water at 270 K. Complete melt-through of a Europan ice shell during cratering would preclude central peak formation. The crater Manannán [Web fig. 2 (*24*)], which is comparable in diameter to Pwyll (Fig. 2F), does not have a well-defined central peak (*23*). This could be the result of an impact into thinner or warmer ice that hindered formation or preservation of a central peak, suggesting that local variations in temperature gradient or ice thickness may exist.

Because several, widely distributed Europan craters exhibit central peaks, our simulations demonstrate that at the times and locations these craters formed, a cold ice layer could not have been as thin as 3 to 4 km. Although complete melt-through of the ice layer does not occur in the simulations with slightly thicker ice, our transient crater sizes are lower limits. Moreover, impacts disrupt target material well beyond the zone of partial melting (*36*), so our simulations put a lower limit on the thickness of the ice. Therefore, we conclude that an ice shell must have been more than 3 to 4 km thick at the times and locations of complex crater formation.

References and Notes

1. P. M. Cassen, S. J. Peale, R. T. Reynolds, in *Satellites of Jupiter*, D. Morrison, Ed. (Univ. of Arizona Press, Tucson, AZ, 1982), pp. 93–128.
2. S. W. Squyres, R. T. Reynolds, P. M. Cassen, S. J. Peale, *Nature* **301**, 225 (1983).
3. M. N. Ross, G. Schubert, *Nature* **325**, 133 (1987).
4. G. W. Ojakangas, D. J. Stevenson, *Icarus* **81**, 220 (1989).
5. P. Helfenstein, E. M. Parmentier, *Icarus* **61**, 175 (1985).
6. A. S. McEwen, *Nature* **321**, 49 (1986).
7. P. E. Geissler *et al.*, *Nature* **391**, 368 (1998).
8. G. V. Hoppa *et al.*, *Icarus* **137**, 341 (1999).
9. P. M. Schenk, W. B. McKinnon, *Icarus* **79**, 75 (1989).
10. M. H. Carr *et al.*, *Nature* **391**, 363 (1998).
11. G. V. Hoppa, B. R. Tufts, R. Greenberg, P. E. Geissler, *Science* **285**, 1899 (1999).
12. M. G. Kivelson *et al.*, *Science* **289**, 1340 (2000).
13. C. Zimmer, K. K. Khurana, M. G. Kivelson, *Icarus* **147**, 329 (2000).
14. J. D. Anderson *et al.*, *Science* **281**, 2019 (1998).
15. R. T. Pappalardo *et al.*, *Nature* **391**, 365 (1998)
16. W. B. McKinnon, *Geophys. Res. Lett.* **26**, 951 (1999).
17. R. Greenberg, P. Geissler, B. R. Tufts, G. V. Hoppa, *J. Geophys. Res.* **105**, 17551 (2000).
18. P. E. Geissler, D. P. O'Brien, R. Greenberg, *Lunar Planet. Sci. Conf.* **XXXII**, 2068 (2001).
19. D. P. O'Brien, P. Geissler, R. Greenberg, *Icarus*, in press.
20. J. A. Rathbun, G. J. Musser Jr., S. W. Squyres, *Geophys. Res. Lett.* **25**, 4157 (1998).
21. R. T. Pappalardo *et al.*, *J. Geophys. Res.* **104**, 24015 (1999).
22. L. M. Prockter, R. T. Pappalardo, *Science* **289**, 941 (2000).
23. J. M. Moore *et al.*, *Icarus* **151**, 93 (2001).
24. Web figures 1 and 2, Web table 1, and text are available at *Science* Online at www.sciencemag.org/cgi/content/full/294/5545/1326/DC1.
25. J. M. Moore *et al.*, *Icarus* **135**, 127 (1998).
26. R. A. F. Grieve, P. B. Robertson, M. R. Dence, *Proc. Lunar Planet. Sci. Conf.* **12A**, 37 (1981).
27. C. M. Pieters, *Science* **215**, 59 (1982).
28. H. J. Melosh, *Impact Cratering: A Geologic Process* (Oxford, New York, 1989).
29. S. L. Thompson, *Tec. Rep. SAND77-1339*, (Sandia National Laboratories, Albuquerque, NM, 1979).
30. S. L. Thompson, H. S. Lauson, *Tec. Rep. SAND89-2951* (Sandia National Laboratories, Albuquerque, NM, 1972).
31. K. Zahnle *et al.*, *Icarus* **136**, 202 (1998).
32. E. Asphaug, W. Benz, *Icarus* **121**, 225 (1996).
33. R. M. Schmidt, K. R. Housen, *Int. J. Impact Eng.* **5**, 543 (1987).
34. Scaling calculations performed using code developed by H. J. Melosh, available at www.lpl.arizona.edu/tekton/crater.html.
35. W. B. Durham, S. H. Kirby, L. A. Stern, *J. Geophys. Res.* **102**, 16293 (1997).
36. H. J. Melosh, *J. Geophys. Res.* **87**, 371 (1982).
37. L. Brookshaw, Working Paper Series SC-MC-9813 (Univ. of Southern Queensland, Queensland, Australia, 1998); available at www.sci.usq.edu.au/cgi-bin/wp/research/workingpapers#1998.

38. Supported by NASA grants NAG5-8937 and NAG-9112. We are indebted to H. J. Melosh, R. D. Lorenz, A. S. McEwen, and L. P. Keszthelyi for helpful discussions and for reviewing the manuscript. We are also grateful to two anonymous reviewers who provided helpful comments.

14 May 2001; accepted 2 October 2001

Centennial-Scale Holocene Climate Variability Revealed by a High-Resolution Speleothem $\delta^{18}O$ Record from SW Ireland

Frank McDermott,[1] David P. Mattey,[2] Chris Hawkesworth[3]

Evaluating the significance of Holocene submillennial $\delta^{18}O$ variability in the Greenland ice cores is crucial for understanding how natural climate oscillations may modulate future anthropogenic warming. A high-resolution oxygen isotope record from a speleothem in southwestern Ireland provides evidence for centennial-scale $\delta^{18}O$ variations that correlate with subtle $\delta^{18}O$ changes in the Greenland ice cores, indicating regionally coherent variability in the early Holocene. Evidence for previously undetected early Holocene cooling events is presented, but mid- to late-Holocene ice rafting in the North Atlantic appears to have had little impact on $\delta^{18}O$ at this ocean margin site.

It is widely accepted that climate variability on time scales of 10^3 to 10^5 years is driven primarily by orbital, or so-called Milankovitch, forcing. Less well understood is the cause of the centennial- to millennial-scale variability that characterizes the $\delta^{18}O$ records of both the glacial and interglacial intervals of the GRIP and GISP2 ice cores (*1*, *2*), yet this higher frequency variability may be important for predicting future climate change. Unlike the last interglacial (isotope stage 5), the Holocene [the last 11,700 years or 11.7 thousand years before the present (ky B.P.)] appeared to be anomalously stable because $\delta^{18}O$ in the GRIP and GISP2 ice cores seemed to be relatively constant (*1*, *2*). More recently, millennial-scale climate variability has been detected in several Holocene climate proxy records, but there is little consensus about the precise timing, amplitude, or cause of these fluctuations (*3–10*). An emerging paradigm is that sub-Milankovitch climate variability is driven by a weak internal quasi-periodic (1500 ± 500 year) forcing of unknown origin that operates irrespective of whether the system is in a glacial or an interglacial mode (*5*, *9*, *10*). In the context of concerns about the impact of anthropogenic greenhouse gases, it is important to establish whether these relatively low-frequency (~1500 year) events or higher frequency oscillations might determine the natural trends in global mean temperatures over the next few centuries. Therefore, a key question is the extent to which subtle higher frequency (century-scale) $\delta^{18}O$ variations in the Holocene sections of the Greenland ice cores reflect regional climatic signals rather than local effects or noise. Until now, that has been difficult to test, due to a paucity of sufficiently high resolution palaeoclimatic records. But here we present a newly found high-resolution O isotope time series for a well-dated stalagmite (CC3) from Crag cave in southwestern Ireland (Fig. 1), which shows that these subtle features are regional and not local signals.

Approximately 1640 laser ablation $\delta^{18}O$ measurements (*11*) were carried out along the growth axis of the 465-mm-long stalagmite, resulting in a high-resolution Holocene $\delta^{18}O$ record (*12–14*). Chronological control is provided by 13 TIMS U-series dates [Web table 1 (*13*)]. Before 5 ky B.P., the resolution is 2 to 20 times better than that of the published (2-m segment) $\delta^{18}O$ data for the GRIP and GISP2 ice cores and is about a factor of two worse than that of the ice cores since 5.3 ky B.P. The average resolution is approximately an order of magnitude better than in the North Atlantic cores that record evidence for quasi-periodic

[1]Department of Geology, University College Dublin, Dublin 4, Ireland. [2]Geology Department, Royal Holloway College, University of London, Egham, Surrey, TW20 OEX, UK. [3]Department of Earth Sciences, Bristol University, Bristol BS8 1RJ, UK.

(1475 ± 500 year) ice rafting during the Holocene (*5*, *9*, *10*). Such events should, therefore, be discernible in the new data set if they had a large impact on the $\delta^{18}O$ of precipitation and/or mean annual air temperatures at this ocean margin site.

The new data are plotted against time (calendar years B.P.) in Fig. 2. $\delta^{18}O$ varies from −11.65 to −0.82 per mil (‰) [Vienna Pee Dee Belemnite (VPDB)], but typically varies by ±1.75‰ around a mean value of −3.26‰ (VPDB). The approximate timing of historic climate variability (*8*) is also shown (e.g., the Little Ice Age, Medieval Warm Period, Dark Ages Cold Period, Roman Warm Period). Colder periods (e.g., Little Ice Age and Dark Ages Cold Period) appear to be associated with lower $\delta^{18}O$ (Fig. 2A). Because $\delta^{18}O$ may be modified by temporal changes in the oceanic moisture source and/or storm track trajectories, it is not possible to calculate temperature changes precisely (*15*). On the basis of present-day spatial $\delta^{18}O$-temperature relations, the magnitude of $\delta^{18}O$ variability around the mean is probably too large to ascribe to changes in air temperature alone. Thus, temperature-driven changes in speleothem $\delta^{18}O$ appear to have been accentuated by synchronous changes in the $\delta^{18}O$ of water vapor supplied to the site, resulting in a strong overall apparent relation between temperature and speleothem $\delta^{18}O$.

Also shown in Fig. 2A (arrows labeled 1 through 6) is the approximate timing of abrupt cooling associated with North Atlantic ice-rafting events (*5*, *9*, *10*). Only event 5 has a clear expression in either the CC3 record (upper curve, Fig. 2A) or in the GISP2 ice core data (lower curve, Fig. 2A). Event 5, the so-called "8200 year cooling event," is defined in CC3 by eight data points centered on 8.32 ± 0.12 ky B.P., and it exhibits a large (~8‰) decrease in $\delta^{18}O$. Event 6 (~9.45 ky B.P.) (*5*) does not have a clear expression in the CC3 record, although it occurs just before several high-amplitude (>4‰) O isotope shifts in the CC3 speleothem record (Fig. 2A). Thus, several shifts to lower $\delta^{18}O$ occur between approximately 9.4 and 8.8 ky B.P., some of which may be recorded in the lower resolution GISP2 record (arrows, Fig. 3). Detection of these events in sediments from the North Atlantic (*5*, *10*) is precluded by the relatively low resolution of the latter records.

The 8200 year event, recognized as the only major Holocene $\delta^{18}O$ event in the GRIP and GISP2 ice cores (*1*, *2*) has been interpreted to reflect a cooling of 7° ± 3°C (*16*). Cooling events dated between 8.4 to 8.0 ky B.P. have also been documented in Europe (*17-21*), North America (*6*, *22*), Northern Canada (*23*, *24*), the Asian and North African moonsonal domains (*25*, *26*), and the equatorial Cariaco Basin (*27*). The timing of the 8200 year event in speleothem CC3 is within the dating uncertainties of the GISP2 core, estimated at ±1 to 2% for this part

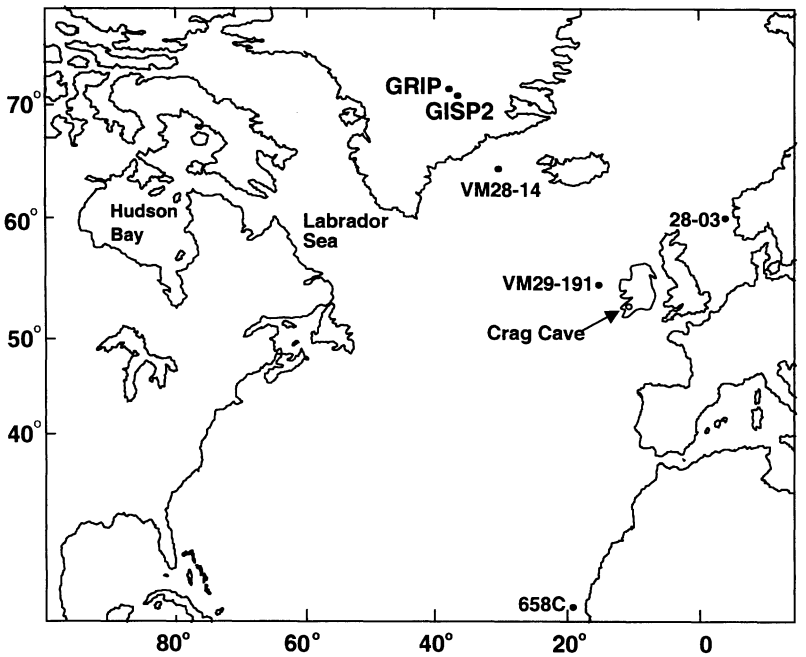

Fig. 1. Map of the North Atlantic region showing the locations of GRIP and GISP2 ice cores, cores VM28-14, VM29-191, 28-03 and Crag Cave in southwestern Ireland.

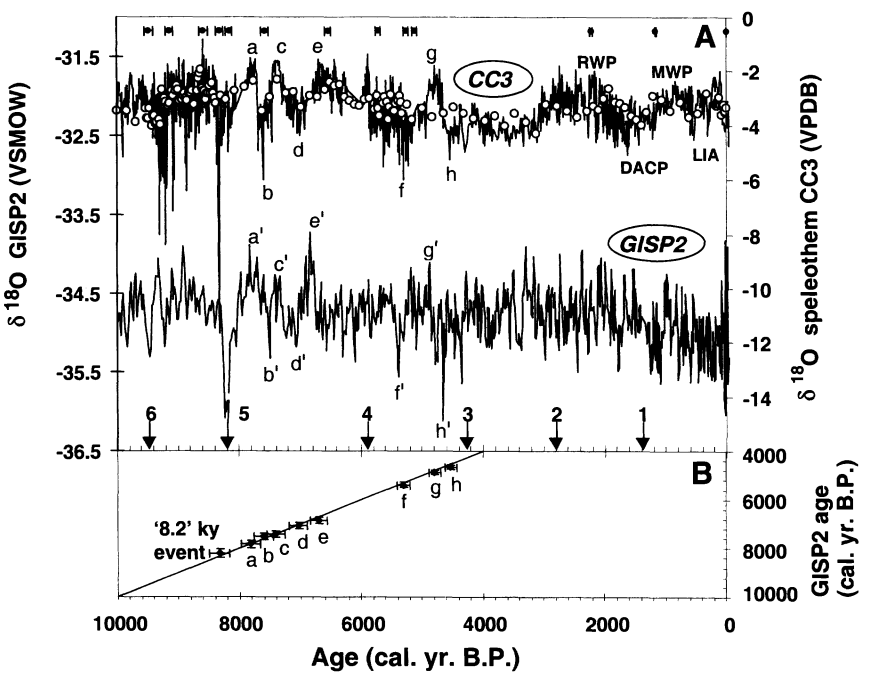

Fig. 2. (**A**) CC3 $\delta^{18}O$ record for the period since 10 ky B.P. (upper curve) compared with the GISP2 record (lower curve). Individual U-Th dates and their ± 1σ error bars are shown in the upper part of the diagram. Open circles represent the published low-resolution conventionally sampled and analyzed $\delta^{18}O$ data (*15*), demonstrating the accuracy of the new laser-ablation data. The 8200 year event was not detected in the conventional $\delta^{18}O$ data because of coarse sampling resolution. The GISP2 curve is the 2-m data set with a resolution of approximately 24 years per $\delta^{18}O$ analysis at 10 ky B.P., increasing to about 7 years per analysis at 0.2 ky B.P. Also shown is the timing of the Bond *et al.* (*5*) ice-rafting events (1 through 6). RWP, Roman Warm Period; DACP, Dark Ages Cold Period; MWP, Medieval Warm Period; LIA, Little Ice Age. Textural and mineralogical descriptions of stalagmite CC3 are given in given in (*15*). (**B**) Timing of events a through h and the 8200 year event in the GISP2 record (y axis) compared with that in CC3 (x axis). Event timing is defined as $\delta^{18}O$ minima or maxima. Error bars shown at ±2.5% for the CC3 chronology and 2.0% for the GISP2 chronology are estimates of dating uncertainties at the 2σ level. The timing of events in both records is identical within the dating uncertainties. Age differences for events range from essentially zero (event a) to 2.6% (event h).

of the Holocene (*28*). Thus, the maximum amplitude occurs at 8.32 ± 0.12 ky B.P. compared with 8.215 ky B.P. in GISP2 and is coeval with faunal evidence for cooling at 8.30 ± 0.06 ky B.P. in core 28-03 from the Norwegian Channel (*17*). Shifts to lower $\delta^{18}O$ between 9.4 and 8.8 ky B.P., detected because of the very high resolution of this part of the record (1 to 3 years per analysis), are interpreted as precursor meltwater release events (*29*) to the catastrophic 8200 year event. The extent to which these centennial-scale changes in $\delta^{18}O$ may be linked to ice-rafting events in the North Atlantic is impossible to assess at present because of the relatively coarse resolution of the latter records (*5*, *10*).

The amplitude of the shift to lower $\delta^{18}O$ at 8.32 ky B.P. (~8‰) is too large to ascribe solely to a reduction in mean annual air temperature (*29*). Instead, we attribute it predominantly to freshening of the surface of the adjacent North Atlantic ocean by isotopically depleted meltwater. Evidence from planktonic foraminifera for a coeval shift in $\delta^{18}O$ in North Atlantic surface waters is equivocal (*5*, *9*, *10*, *30*), possibly because enrichments in $\delta^{18}O$ were offset by the lower $\delta^{18}O$ values of waters derived from melting drift-ice or because of a change in depth habitat in response to surface cooling (*5*, *10*). The chronology of our new record is consistent with suggestions (*19*, *24*) that the 8200 year event was triggered by a catastrophic release of meltwaters by sudden draining of large ice-dammed lakes on the margins of the Laurentide ice sheet in northeastern Canada (*31*), dated to 8.47 ± 0.30 ky B.P. (*24*). The absence of a clear shift in $\delta^{18}O$ in the speleothem data during the other North Atlantic ice-rafting events at about 5.9, 4.3, 2.8, and 1.4 ky B.P. (*5*), despite the high resolution of the new data (7 to 18 years per analysis), is important. It suggests that unlike the 8200 year event, the later Holocene ice rafting events (*5*, *10*) failed to trigger large changes in $\delta^{18}O$ and, by implication, may not have established a detectable meltwater cap on the mid-latitude North Atlantic (*29*).

Although precise comparisons between the GISP2 and CC3 records are hampered by dating uncertainties, the low amplitude of the variations, and differences in sampling resolution, the subtle pattern of $\delta^{18}O$ variability between approximately 8.4 and 4.5 ky B.P. is strikingly similar in both records (Fig. 2A). Excluding the 8200 year event, which is clearly common to both records, approximately eight peaks and troughs may be correlated within the combined dating uncertainties in this time interval (labeled a through h, Fig. 2A). Figure 2B illustrates that the timing of each event coincides in both records within the dating uncertainties. Cooling events b, d, f, and h (Fig. 2A) may reflect weaker North Atlantic thermohaline overturning at 7.73, 7.01, 5.21, and 4.2 ky B.P., respectively (*8*). We interpret these covariations to mean that the subtle $\delta^{18}O$ variability in the early and mid-Holocene sections of the Greenland ice cores reflects coherent climate-driven in-phase changes in the $\delta^{18}O$ of precipitation over a large region around the eastern North Atlantic margin. Differences in the shape of individual peaks and troughs are attributed to second-order effects such as temporal changes in the vapor source, trajectory, and rainout efficiency of clouds supplying moisture to these sites. The GISP2 and CC3 data appear to be decoupled in the latter part of the Holocene, but the CC3 data exhibit variations that are broadly consistent with a Medieval Warm Period (MWP) at ~1000 ± 200 years ago and a two-stage Little Ice Age (LIA), as reconstructed by inverse modeling of temperature profiles in the Greenland Ice Sheet (*32*).

The coherent $\delta^{18}O$ variations in CC3 and GISP2 (events a through h, Fig. 2A) indicate that many of the subtle multicentury $\delta^{18}O$ variations in the Greenland ice cores reflect regional North Atlantic margin climate signals rather than local effects. Spectral analysis of the data confirms the importance of multicentury variability with peaks centerd on 625, 169, and 78 years. Taken together with historically documented variability (e.g., LIA and MWP in Fig. 2A) we argue that high-frequency (centennial-scale) oscillations, perhaps reflecting North Atlantic thermohaline circulation changes (*8*, *33*) may have a more detectable impact on the climates of North Atlantic ocean-margin sites than the lower frequency events exquisitely recorded by ice-rafting proxies.

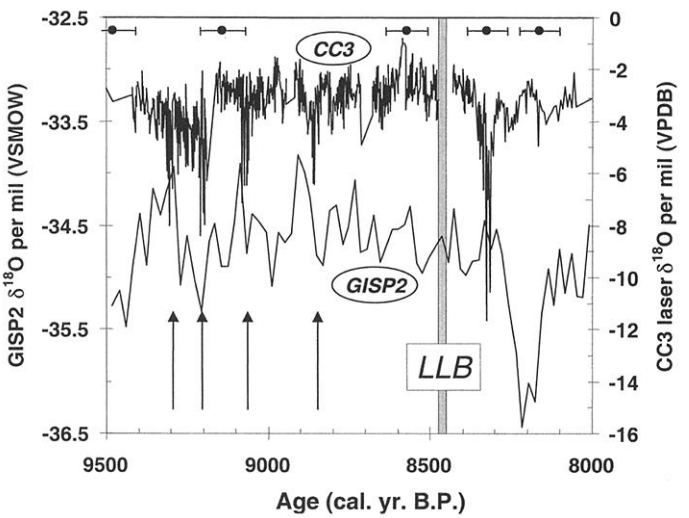

Fig. 3. Close up of period between 9500 and 8000 years showing the new laser ablation CC3 record (upper curve) and the GISP2 curve. The vertical shaded line at 8470 years B.P. labeled LLB denotes the approximate timing of the Laurentide Lakes Burst event (*24*). U-series ages and their 1σ error bars are shown in the upper part of the diagram. Arrows denote timing of $\delta^{18}O$ fluctuations in the new high-resolution record, interpreted as meltwater release events.

References and Notes

1. W. Dansgaard *et al.*, *Nature* **364**, 218 (1993).
2. P. M. Grootes, M. Stuiver, J. W. C. White, S. J. Johnsen, J. Jouzel, *Nature* **366**, 552 (1993).
3. P. A. Mayewski *et al.*, *J. Geophys. Res.* **102**, 26345 (1997).
4. R. B. Alley *et al. Geology* **25**, 483 (1997).
5. G. Bond *et al. Science* **278**, 1257 (1997).
6. I. D. Campbell, C. Campbell, M. J. Apps, N. W. Rutter, A. B. G. Bush, *Geology* **26**, 471 (1998).
7. F. S. Hu, H. E. Wright, E. Ito, K. Lease, *Nature* **400**, 437 (1999).
8. G. G. Bianchi, I. N. McCave, *Nature* **397**, 515 (1999).
9. P. DeMenocal, J. Ortiz, T. Guilderson, M. Sarnthein, *Science* **288**, 2198 (2000).
10. G. Bond *et al.*, in *Mechanisms of Global Climate Change at Millennial Scales*. P. U. Clark, R. S. Webb, L. D. Keogwin, Eds. (Geophysical Monograph Series, American Geophysical Union, Washington, DC, 1999), vol. 12, pp. 35–58.
11. D. P. Mattey, M. Brownless, Isotopes in Palaeoclimate Research, Abs. Vol. Conf. Leicester University (April 1999).
12. The laser ablation–gas chromatography–isotope ratio mass spectrometry (LA-GC-IRMS) system uses a 25-W CO_2 laser heat source with a continuous helium flow sample chamber to a gas chromatograph (GC) and mass spectrometer (MS). CO_2 is thermally released by 400-ms laser bursts (beam diameter, approximately 150 μm) and is swept through a 80-cm packed GC column into the MS for isotope analysis, relative to a pulse of reference gas injected at the start of the run. Analysis of Cararra marble and other standards gives similar $\delta^{13}C$ values to those obtained by conventional acid digestion, but $\delta^{18}O$ values that are systematically lowered by 2‰. Replicate analyses of standards indicate that the isotope data are reproducible to better than 0.1‰ for $\delta^{13}C$ and 0.2‰ for $\delta^{18}O$. Using a system of forward and reverse profiling along the central growth axis of the stalagmite, a spatial resolution of 250 μm was achieved. After the 2‰ correction, the new data accurately reproduce the first-order features of the coarse resolution O isotope record for this speleothem (open circles, Fig. 2A) constructed previously by dental-drill sampling and conventional gas-source MS. Previous work has shown that O isotopes were incorporated in isotopic equilibrium with the cave drip-waters (*15*).
13. Web table 1 is available at *Science* Online at www.sciencemag.org/cgi/content/full/294/5545/1328/DC1. Ages were assigned by linear interpolation between the dated intervals.
14. For the latter part of the Holocene (since 5500 calendar years ago), each O isotope analysis represents 10 to 22 years, but the resolution is sub-decadal for all of the period before 5300 years ago, reflecting higher speleothem growth rates.
15. F. McDermott *et al. Quat. Sci. Rev.* **18**, 1021 (1999).
16. K. M. Cuffey, R. B. Alley, P. M. Grootes, J. M. Bolzan, S. Anandakrishnan, *J. Glaciol.* **40**, 341 (1994).
17. D. Klitgaard-Kristensen, H. P. Sejrup, H. Haflidason, S. Johnsen, M. Spurk, *J. Quat. Sci.* **13**, 165 (1998).
18. D. R. Rousseau, R. Precce, N. Limondin-Lozouet, *Geology* **26**, 651 (1998).
19. U. von Grafenstein, H. Erlenkeuser, J. Muller, J. Jouzel, S. Johnsen, *Clim. Dyn.* **14**, 73 (1998).
20. A. Korhola, J. Weckstrom, *Quat. Res.* **54**, 284 (2000).
21. A. Nesje, S. O. Dahl, *J. Quat. Sci.* **16**, 155 (2001).
22. W. E. Dean, *Geol. Soc. Am. Spec. Pap.* **276**, 135 (1993).
23. D. A. Fisher, R. M. Koerner, N. Reeth, *Holocene* **5**, 19 (1995).

24. D. C. Barber *et al. Nature* **400**, 344 (1999).
25. F. A. Street-Perrott, R. A. Perrott, *Nature* **358**, 607 (1990).
26. F. Sirocko *et al., Nature* **364**, 322 (1993).
27. K. Hugen, J. T. Overpeck, L. C. Peterson, S. Trumbore, *Nature* **380**, 51 (1996).
28. R. B. Alley *et al. J. Geophys. Res.* **102**, 26367 (1997).
29. The temperature dependence of $\delta^{18}O$ in precipitation varies in space and time, but if air temperature was the only variable responsible, a decrease of approximately 20°C would be required to explain the 8‰ decrease. This is based on the average $d\delta^{18}O/dT$ relation in modern precipitation (~0.6‰ °C^{-1}), and the water-calcite fractionation that accompanies speleothem deposition (~−0.24‰ °C^{-1}). Because the mean annual air temperature of the region is 10.4°C and speleothem deposition continued through the event, changes in air temperature alone cannot account for a $\delta^{18}O$ shift of this magnitude. Similar arguments apply to the lower amplitude events between 9.4 and 8.8 ky B.P. (Fig. 3).
30. J. C. Duplessy, E. Bard, L. Labeyrie, J. Duprat, J. Moyes, *Paleoceanography* **8**, 341 (1993).
31. P. U. Clark, W. W. Fitzhugh, *Quat. Res.* **34**, 296 (1990).
32. D. Dahl-Jensen *et al., Science* **282**, 268 (1998).
33. H. W. Arz, S. Gerhardt, J. Pätzold, U. Röhl, *Geology* **29**, 239 (2001).
34. We gratefully acknowledge the assistance of M. Brownless during the course of this study. M. Gilmour (Open University) is thanked for providing the four new TIMS U-Th dates. We thank the cave owners at Crag for their enthusiastic cooperation. We thank G. Bond and an anonymous reviewer for constructive reviews.

21 June 2001; accepted 17 September 2001

Trithorax and dCBP Acting in a Complex to Maintain Expression of a Homeotic Gene

Svetlana Petruk,[1]* Yurii Sedkov,[1]* Sheryl Smith,[1] Sergei Tillib,[1] Vladislav Kraevski,[1] Tatsuya Nakamura,[1] Eli Canaani,[1,2] Carlo M. Croce,[1] Alexander Mazo[1]†

Trithorax (Trx) is a member of the trithorax group (trxG) of epigenetic regulators, which is required to maintain active states of Hox gene expression during development. We have purified from *Drosophila* embryos a trithorax acetylation complex (TAC1) that contains Trx, dCBP, and Sbf1. Like CBP, TAC1 acetylates core histones in nucleosomes, suggesting that this activity may be important for epigenetic maintenance of gene activity. dCBP and Sbf1 associate with specific sites on salivary gland polytene chromosomes, colocalizing with many Trx binding sites. One of these is the site of the Hox gene *Ultrabithorax* (*Ubx*). Mutations in either *trx* or the gene encoding dCBP reduce expression of the endogenous *Ubx* gene as well as of transgenes driven by the *bxd* regulatory region of *Ubx*. Thus Trx, dCBP, and Sbf1 are closely linked, physically and functionally, in the maintenance of Hox gene expression.

In *Drosophila*, trxG genes are required to sustain appropriate levels of Hox gene expression during embryogenesis. Several proteins of the trxG are constituents of SWI/SNF-type chromatin remodeling complexes (*1, 2*), which suggests that some of these proteins exert their regulatory effects through alterations in chromatin structure. The mode of action of other trxG proteins, including Trx, is not known.

To investigate the function of trxG proteins, we purified a Trx protein complex from *Drosophila* embryos. To monitor the purification, we used the Trx antibody N1, which has been characterized previously (*3, 4*). Nuclear extract was fractionated using several chromatographic steps (*5*) (Fig. 1A). Three prominent bands are seen in the purified material, which contains most of the Trx found in the starting extract (Fig. 1B). We refer to this complex as trithorax acetylation complex 1 (TAC1). We estimate the size of TAC1 to be 1 MD, as determined from size fractionation of the highly purified 0.25 M Q Sepharose material on a 20 to 45% glycerol gradient (Fig. 1D). All three TAC1 components co-migrated on this gradient, as assayed by silver staining (*6*). No lower molecular weight proteins were detected in the purified material. The higher molecular weight band in TAC1 was recognized by N1 (Fig. 1C). In addition to Trx, two similar sized bands of about 300 kD were detected (Fig. 1B). The purified material was resolved by SDS–polyacrylamide gel electrophoresis (PAGE), and the protein bands were excised, digested with trypsin, and analyzed by mass spectrometry (*5*). This analysis confirmed that the upper band is Trx. Results from other bands showed that the upper band in the doublet is the *Drosophila* acetyltransferase dCBP and the lower band is Sbf1. Sbf1 is a mammalian anti-phosphatase that was previously found to interact with the SET (Suvar3-9, Enhancer-of-zeste, Trithorax) domain of ALL-1/HRX/MLL (*7*), the human homolog of Trx, which is known to be involved in acute leukemia.

To confirm these results, we raised specific antibodies to dCBP (C2) and Sbf1 (S1) (*8*), which detected single protein bands of the expected sizes in the purified material (Fig. 1C). Using these antibodies, we found that a portion

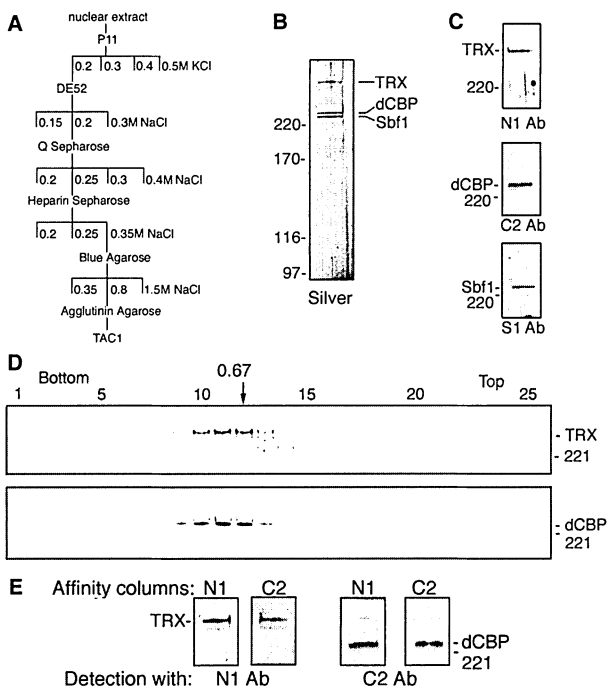

Fig. 1. Trx and dCBP are components of the TAC1 complex. **(A)** The TAC1 purification scheme. **(B)** Silver staining of material from an agglutinin–Agarose column. **(C)** Western blots of Trx, dCBP, and Sbf1 after fractionation on an agglutinin–Agarose column. **(D)** The 0.25 M NaCl Q Sepharose fraction was size-fractionated by glycerol gradient. Trx and dCBP proteins were visualized by Western blotting of the same filter. The position of the 670 kD protein marker is indicated. **(E)** The material from peak fractions of the glycerol gradient was applied independently to columns with attached antibodies to Trx (N1) and dCBP (C2). Eluted material was separated by 6% SDS-PAGE and used for Western blotting.

[1]Kimmel Cancer Center, Thomas Jefferson University, Philadelphia, PA 19107, USA. [2]Department of Molecular Cell Biology, Weizmann Institute of Science, Rehovot 76100, Israel.

*These authors contributed equally to this work.
†To whom correspondence should be addressed. E-mail: A_Mazo@lac.jci.tju.edu